Journal of Electronic Imaging

JElectronicImaging.org

Robust maximum *a posteriori* image super-resolution

Michalis Vrigkas
Christophoros Nikou
Lisimachos P. Kondi

SPIE. IS&T imaging.org

Robust maximum *a posteriori* image super-resolution

Michalis Vrigkas,* Christophoros Nikou, and Lisimachos P. Kondi
University of Ioannina, Department of Computer Science & Engineering, Ioannina 45110, Greece

Abstract. A global robust M-estimation scheme for maximum *a posteriori* (MAP) image super-resolution which efficiently addresses the presence of outliers in the low-resolution images is proposed. In iterative MAP image super-resolution, the objective function to be minimized involves the highly resolved image, a parameter controlling the step size of the iterative algorithm, and a parameter weighing the data fidelity term with respect to the smoothness term. Apart from the robust estimation of the high-resolution image, the contribution of the proposed method is twofold: (1) the robust computation of the regularization parameters controlling the relative strength of the prior with respect to the data fidelity term and (2) the robust estimation of the optimal step size in the update of the high-resolution image. Experimental results demonstrate that integrating these estimations into a robust framework leads to significant improvement in the accuracy of the high-resolution image. *© 2014 SPIE and IS&T* [DOI: 10.1117/1.JEI.23.4.043016]

Keywords: maximum a posteriori; image super-resolution; robust M-estimator; Tikhonov regularization.

Paper 14253 received Apr. 29, 2014; revised manuscript received Jun. 17, 2014; accepted for publication Jun. 27, 2014; published online Jul. 31, 2014.

1 Introduction

Image super-resolution (SR) is a technique for enhancing the quality and the resolution of an image. The objective is to improve the spatial resolution by using information from a set of several different low-resolution (LR) images to produce an image with more visible detail in the high spatial frequency features. The LR images may experience different degradations, such as motion, point spread function blurring, subsampling, and additive noise. The reconstructed high-resolution (HR) image can be successfully estimated if subpixel shifts exist between the LR images. In this manner, each frame of the LR sequence brings complementary information to the original HR image.

Researchers studying the direct inverse solution recognized the limitations of the problem which is ill-posed due to interpolation, motion compensation, inverse filtering, and additive noise.[1–3] Even in the cases of perfect motion registration and accurate knowledge of the point spread function of the acquisition system, a significant dependence of the estimation of the HR image on degradation conditions is observed. A large family of SR methods is based on a stochastic formulation of the problem, which imposes a prior distribution on the image to be reconstructed and provides estimates in a maximum *a posteriori* (MAP) framework where the posterior distribution of the HR image is maximized.[1–9] In the same context, Bayesian approaches have also been proposed in the literature.[7,10–14]

More recent approaches have shown great potential in recognizing a human face by applying SR techniques. The work of Bilgazyev et al.[15] recognizes human faces by learning the high-frequency components of facial images and applying them to the LR images in order to create an HR image. Baker and Kanade[16] use a prior on a spatial distribution of facial images in order to produce an HR image. A Bayesian approach for image SR from a single image is proposed by Tappen and Liu.[17] This method is an alignment-based approach that leverages facial LR images. A novel approach that models super-resolved faces in three-dimensional (3-D) space is presented by Berretti et al.[18] 3-D scans of LR images are aligned in order to produce an HR 3-D face model called "superface."

Violations of the assumptions of data fidelity to the assumed model are also likely to occur because SR methods are very sensitive to inaccuracies of their parameters. However, little has been reported about suppressing the outlier artifacts (i.e., salt and pepper noise, misregistration errors, and occlusion). For instance, median filters have been efficiently used to treat the SR problem[19] where robustness is introduced by applying a median filter in each term of a backprojected difference image.

In the same context, a robust color image SR algorithm has previously shown great potential for estimating HR images with crisp details.[20–22] A comparative study of M-estimators for image SR was presented by El-Yamany and Papamichalis.[20] The main concern of this study is to provide a comparison of the trade-off between the estimator robustness and the edge preservation of the highly resolved image. In a preliminary work, a robust image SR estimation was introduced. The use of an L_1 error norm in the objective function provides a good framework for removing the outliers from the LR images. The work of El-Yamany and Papamichalis[22] introduced a robust error norm in the objective function. The iterative reconstruction process is repeated for every LR image, suppressing the outliers without the use of a regularization term in the objective function. An independent effort for reducing the aliasing artifacts in a multiframe SR framework using deblurring algorithms is proposed by Robinson et al.[23]

Much research has focused on stochastic techniques in an MAP framework.[24,25] Patanavijit et al.[25] used a Huber error norm for measuring the difference between the estimation of an HR image and each LR image. A factor that affects the SR quality is also the Tikhonov regularization term, which is

*Address all correspondence to: Michalis Vrigkas, E-mail: mvrigkas@cs.uoi.gr

used to remove artifacts from the final solutions. Based on a stochastic Bayesian approach, the work of Patanavijit et al.[24] performs image SR by minimizing a cost function. The Lorentzian error norm is utilized in order to measure the difference between the estimated HR image (projected onto the LR grid) and each LR image. The authors combine the Tikhonov and the Lorentzian error norms and use the combiination as a regularizer to remove artifacts from the final solution and improve the convergence rate.

The work of Tanaka et al.[26] addresses the problem of estimating an HR image in a robust framework. The authors provide an accurate algorithm for extracting single-motion regions and their registration parameters, where the whole algorithm is executed in three steps. In the first step, the algorithm estimates the motion parameters between the LR images and the reference (current HR estimation) image. Then, the region associated with the registration parameters is extracted, and finally, the algorithm defines the registration parameters inside the motion region.

Robust image SR algorithms are usually sensitive to their assumed model of data and noise. The work of Farsiu et al.[27] introduces an L_1 norm minimization approach for robust image SR using a bilateral prior as a regularizer in order to deal with different data and noise models. This approach preserves the edges of the highly resolved image, however, it is fast but is prone to motion errors, blur, and outliers.

The main contribution of this work is the employment of a fully robust image SR technique combined with an MAP framework. The objective function to be minimized employs a regularization term, which controls the smoothness of the reconstructed highly resolved image. The regularization parameters and the optimal step size of the update equation are computed using robust M-estimators in contrast to previous works,[22,24] which employ robust M-estimators only in the estimation of the HR image. Both the regularization parameters and the optimal step size are computed in a closed form from the input data, thus providing more robustness to the estimation of the highly resolved image by retaining crisp details and fully removing the outliers. The proposed method can efficiently reconstruct an HR image from several LR images, which suffer from salt and pepper noise, speckle noise, large misregistration errors, and occlusion. A four-page summary of this work was presented by Vrigkas et al.[28] Experiments show that the reconstructed HR image is of higher quality than that in the standard MAP-based methods[22,24] employing robust estimation only for the estimation of the HR image.

2 Image Formation Model

The image degradation process[3] is modeled by motion (rotation and translation), a linear blur, and subsampling by pixel averaging along with additive Gaussian noise. We assume that p LR images, each of size $M = N_1 \times N_2$, are obtained from the acquisition process. The following observation model is assumed, where all images are ordered lexicographically

$$\mathbf{y} = \mathbf{W}\mathbf{z} + \mathbf{n}. \tag{1}$$

The set of LR frames is described as $\mathbf{y} = [\mathbf{y}_1^T, \mathbf{y}_2^T, \ldots, \mathbf{y}_p^T]^T$, where $\mathbf{y}_k$, for $k = 1, \ldots p$, are the p LR images. The desired HR image $\mathbf{z}$ is of size $N = l_1 N_1 \times l_2 N_2$, where l_1 and l_2 represent the upsampling factors in the horizontal and vertical directions, respectively. The term n represents zero-mean additive Gaussian noise. In Eq. (1), the degradation matrix $\mathbf{W} = [\mathbf{W}_1^T, \mathbf{W}_2^T, \ldots, \mathbf{W}_p^T]^T$ performs the operations of motion, blur, and subsampling. Thus, matrix $\mathbf{W}_k$, for the k'th frame, may be written as

$$\mathbf{W}_k = \mathbf{D}\mathbf{B}_k\mathbf{M}(\mathbf{s}_k), \tag{2}$$

where $\mathbf{D}$ is the $N_1 N_2 \times N$ subsampling matrix, $\mathbf{B}_k$ is the $N \times N$ blurring matrix, and $\mathbf{M}(\mathbf{s}_k)$ is the $N \times N$ rigid transformation matrix with parameters (rotation angle and translation vector) denoted by $\mathbf{s}_k$ for the k'th frame. Finally, $\mathbf{n}$ is additive Gaussian noise.

A regularized approach using the image prior information of the HR image (Gaussian assumption) can be used to make the inverse problem well-posed. Considering that each LR image may result from a different degradation process, which implies that a different weighting should be given to it in the desired solution, the following channel-weighted cost function is proposed:[2]

$$L(\mathbf{z}, \mathbf{s}) = \sum_{k=1}^{p} \|\mathbf{y}_k - \mathbf{W}_k(\mathbf{s}_k)\mathbf{z}\|^2 + \alpha_k(\mathbf{z})\|\mathbf{Q}\mathbf{z}\|^2, \tag{3}$$

where Q is a matrix applying a high-pass filter (in our case the Laplacian) and penalizes discontinuities in the final solution. The regularization parameters $\alpha_k(\mathbf{z})$ control the relative contribution between the error term for the k'th LR image (residual norm $||\mathbf{y}_k - \mathbf{W}_k(\mathbf{s}_k)\mathbf{z}||^2$) and the smoothness norm $||\mathbf{Q}\mathbf{z}||^2$. In Eq. (3), it is implied that the registration $\mathbf{s}_k$ parameters are collected in $\mathbf{s}$ in this type of formulation.

3 Robust Image Super-Resolution

In our previous work,[2] it has been shown that the regularization parameters $\alpha_k(\mathbf{z})$ may be obtained in closed form from the images.

$$\alpha_k(\mathbf{z}) = \frac{||\mathbf{y}_k - \mathbf{W}_k\mathbf{z}||^2}{2||\mathbf{y}_k||^2 - ||\mathbf{Q}\mathbf{z}||^2}, \tag{4}$$

where we have omitted the dependence of matrix $\mathbf{W}_k$ on the registration parameters $\mathbf{s}_k$ to simplify the notation.

Estimation of the registration parameters $\mathbf{s}$ and the HR image $\mathbf{z}$ may be obtained by an alternating optimization scheme.[1–3] In a first step, the registration parameters may be computed by a variety of methods involving block matching schemes[1–3] or algorithms combining feature extraction and mutual information.[8] Having fixed the registration parameters, we may use a gradient descent method with a properly calculated step size to minimize Eq. (3) with respect to the HR image.

$$\hat{\mathbf{z}}^{n+1} = \hat{\mathbf{z}}^n - \varepsilon^n g(\hat{\mathbf{z}})^n,$$

$$\hat{\mathbf{z}}^{n+1} = \hat{\mathbf{z}}^n - \sum_{k=1}^{p} \varepsilon_k^n \mathbf{W}_k^T(\mathbf{W}_k\hat{\mathbf{z}}^n - \mathbf{y}_k) + \alpha_k(\mathbf{z})\left\|\mathbf{Q}\mathbf{z}\right\|^2. \tag{5}$$

The parameter ε^n is the step size at the n'th iteration, which may be obtained in closed form directly from the image data[1] by

$$\varepsilon_k^n = \frac{\sum_{m=1}^{pM} [\mathbf{Wg}]_m [(\mathbf{W}_k\mathbf{z} - \mathbf{y}_k)]_m + \sum_{k=1}^{p} \alpha_k(\mathbf{z}) \sum_{i=1}^{N} [\mathbf{Qg}(\mathbf{z})]_i [\mathbf{Qz}]_i}{\sum_{m=1}^{pM} [\mathbf{Wg}]_m^2 [(\mathbf{W}_k\mathbf{z} - \mathbf{y}_k)]_m^2 + \sum_{k=1}^{p} \alpha_k(\mathbf{z}) \sum_{i=1}^{N} [\mathbf{Qg}(\mathbf{z})]_i}, \tag{6}$$

where the operator $[\cdot]_i$ takes the i'th element of the vectorized matrix inside the brackets.

SR reconstruction is an ill-posed inverse problem due to the existence of the additive noise. In order to stabilize the inversion process in cases of non-Gaussian noise, we introduce an SR algorithm that uses robust error norm in the data fidelity term of the objective function. This approach is based on the class of robust M-estimators. The objective function uses a regularization term that can help the SR algorithm to remove any artifacts from the final solution. We are interested in estimators whose influence function is differentiable and bounded, such as the Lorentzian estimator, defined as

$$\rho(x,\sigma) = \log\left[1 + \frac{1}{2}\left(\frac{x}{\sigma}\right)^2\right] \quad \psi(x,\sigma) = \frac{2x}{2\sigma^2 + x^2}, \tag{7}$$

where σ is the scale factor and ψ is the influence function, defined as the first derivative of the robust estimator ρ.

The scale factor controls a threshold beyond which all points are considered to be outliers. Violations in the mathematical model in Eq. (1) and, consequently, in the data term in Eq. (3) may yield large errors, which can severely influence the reconstruction process. The choice of the scale factor σ plays a crucial role in controlling the outliers. Errors falling beyond that threshold are assigned smaller weights and the corresponding outlying measures are suppressed. For small values of the scale factor, the influence function decreases faster, assigning smaller weights to errors that outstrip the value of this parameter. If the value of σ is relatively small, the contribution of the LR frames will be canceled, leading to a bad estimation of the HR image due to the insufficient information provided by the LR frames. On the other hand, if the value of the scale factor is chosen to be arbitrarily large, outliers will significantly contribute to the estimation of the HR image. El-Yamany and Papamichalis[22] have presented a method for calculating the outlier threshold which is based on the similarity between a reference LR frame and the k'th motion-compensated LR frame.

Formulating the observation model of Eq. (1) in an M-estimation framework, the solution for the HR image is obtained by the following minimization problem:

$$\mathbf{z}^* = \arg\min_{\mathbf{z}} \left\{ \sum_{i=1}^{M} [\rho(\mathbf{W}_k\mathbf{z} - \mathbf{y}_k; \sigma_k)]_i + \alpha_k(\mathbf{z}) \|\mathbf{Qz}\|^2 \right\}. \tag{8}$$

Note that in Eq. (8) different outlier thresholds are assigned to different LR frames.

Following the calculation of the regularization term in Eq. (4), the robust regularization parameter determining the trade-off between the fidelity of the observed data and the image prior now becomes

$$\alpha_k(\mathbf{z}) = \frac{\sum_{i=1}^{M} [\rho(\mathbf{y}_k - \mathbf{W}_k\mathbf{z}; \sigma_k)]_i^2}{2\|\mathbf{y}_k\|^2 - \|\mathbf{Qz}\|^2}. \tag{9}$$

To obtain a robust solution of Eq. (8), the gradient descent scheme of Eq. (6) is transformed to its robust counterpart.

$$\hat{\mathbf{z}}^{n+1} = \hat{\mathbf{z}}^n - \sum_{k=1}^{p} \varepsilon_k^n \mathbf{W}_k^T \psi(\mathbf{W}_k\hat{\mathbf{z}}^n - \mathbf{y}_k; \sigma_k) + \alpha_k(\mathbf{z}) \|\mathbf{Qz}\|^2, \tag{10}$$

where the influence function ψ of the robust estimation is now involved.

It must be noted that the choice of the step-size parameter ε_k^n plays an important role in the behavior of the gradient descent method. This parameter must be small enough to prevent divergence and large enough to provide fast convergence. A constant step size could be the easiest solution, but this is an inappropriate approach for most of the robust image SR problems. After some manipulation, following the spirit of the approach,[1] a robust closed form solution of the optimal step size may be obtained.

$$\varepsilon_k^n = \frac{\sum_{m=1}^{pM} [\mathbf{Wg}]_m [\psi(\mathbf{W}_k\mathbf{z} - \mathbf{y}_k; \sigma_k)]_m + \sum_{k=1}^{p} \alpha_k(\mathbf{z}) \sum_{i=1}^{N} [\mathbf{Qg}(\mathbf{z})]_i [\mathbf{Qz}]_i}{\sum_{m=1}^{pM} [\mathbf{Wg}]_m^2 [\rho(\mathbf{W}_k\mathbf{z} - \mathbf{y}_k; \sigma_k)]_m^2 + \sum_{k=1}^{p} \alpha_k(\mathbf{z}) \sum_{i=1}^{N} [\mathbf{Qg}(\mathbf{z})]_i}. \tag{11}$$

Note that both the robust estimator ρ and its influence function ψ appear in Eq. (11).

This optimal step size [Eq. (11)] is calculated for every single LR image. Having an adaptive step size provides a better convergence and also keeps the algorithm from trapping into erroneous solutions.

In robust image SR reconstruction, it is necessary to define a process for automatically computing the value of the outlier threshold parameter. In statistics, the median absolute deviation (MAD) criterion[29] is considered to be one of the most accurate robust measures of the variability of a univariate sample of quantitative data. For the k'th LR image,

$$\mathrm{MAD}_k^n = \underset{i}{\mathrm{median}}\{|r_{k,i}^n([\mathrm{W}_k z^{n-1}; y_k]_i) - \underset{j}{\mathrm{median}}(r_{m,j}^n([\mathrm{W}_m z^{n-1}; y_m)]_j)|\}, \tag{12}$$

where $n = 0,1,2,\ldots$ refers to the n'th iteration of the algorithm and

$$r_{k,i}^n(\mathbf{W}_k\mathbf{z}^{n-1}; \mathbf{y}_k) = [\mathbf{W}_k\mathbf{z}^{n-1} - \mathbf{y}_k]_i \tag{13}$$

is the residual error of the i'th datum between the estimation of the degraded HR image and the k'th LR frame. MAD is a measure of statistical dispersion. It is a robust statistic, being

Algorithm 1 Robust super-resolution image reconstruction algorithm.

Input: Low-resolution images $\mathbf{y}_k, k = 1,2, \cdots, p$.

Output: High-resolution image estimate $\hat{\mathbf{z}}^n$.

- First estimate of the HR image $\hat{\mathbf{z}}^0$ using Eq. (10).
- Initial estimate of scale factor σ_k^0 with the median of the residual errors for $k = 1,2, \cdots, p$.
- Register the upscaled $\mathbf{y}_k$ to $\hat{\mathbf{z}}^0, k = 1,2, \cdots, p$;[8] $n := 1$;
- **do**
  - **do**
    * Random selection of an LR image $\mathbf{y}_k$.
    * **if** $\mathbf{y}_k$ is visited
      - Compute the robust regularization parameter $\alpha_k(\hat{\mathbf{z}}^n)$ using Eq. (9).
      - Estimate the optimal step size ε_k^n according to Eq. (11).
      - Compute scale factor σ_k^n given in Eq. (14).
      - Update $\hat{\mathbf{z}}^n$ using Eq. (10).
    * **end**
    * Declare $\mathbf{y}_k$ visited.
  - **until all** $\mathbf{y}_k$ are visited.
  - $n := n + 1$;
  - Declare all $\mathbf{y}_k, k = 1, \ldots p$ unvisited.
- **until** or a predefined number of iterations is reached.

more resilient to outliers in a data set. In order to use MAD criterion as a consistent estimator for the estimation of the scale factor, we consider $\sigma_k^n = K \cdot \mathrm{MAD}_k^n$, where K is a constant that depends on the distribution. For normally distributed data with standard deviation 1, $K = 1/\Phi^{-1}(3/4) \approx 1.4826$, where Φ^{-1} is the inverse of the cumulative distribution function for the standard normal distribution.[29] In that case, for the k'th LR frame, the scale factor σ_k is computed as follows:

$$\sigma_k^n = 1.4826 \cdot \mathrm{MAD}_k^n, k = 1,2, \cdots, p. \tag{14}$$

The scale factor σ_k^n is obtained in an automatic way according to Eq. (14) from all the LR frames. In general, the estimation of σ_k^n depends on the similarity between the k'th LR frame and the degraded estimation of the HR image at the n'th iteration. Thus, the scale factor is computed as the median of the residuals. The overall algorithm is summarized in Algorithm 1.

Following a similar approach, El-Yamany and Papamichalis[22] introduced the Lorentzian estimator [Eq. (7)] to minimize the objective function and estimate the HR image. They developed a heuristic way of computing the scale factor as a function of the ground truth image and the estimated highly resolved image. Moreover, their step size was defined to be half of the scale factor value. The Tikhonov regularization has also been used in order to obtain a fine solution for the three channels of color.

The Lorentzian M-estimator is a very popular estimator among image reconstruction techniques. The work of Patanavijit et al.[24] combines the Lorentzian estimator with a Laplacian regularization function in order to find a solution to the problem of SR. In their work, the choice of the scale factor, the step size, and the regularization parameter is heuristic.

4 Experimental Results

In order to evaluate the proposed methodology, four different sets of experiments were conducted on synthetic data sets. Sequences of LR images were created by blurring, downsampling, and degrading by noise an original image. At first, the images were downsampled by a factor of 2 (4 pixels to 1). Then, a point spread function of a 5×5 Gaussian kernel with standard deviation of 1 was applied and the resulting images were degraded by white Gaussian noise in order to obtain a signal-to-noise ratio of 30 dB.

To highlight the importance of the proposed fully robust ST scheme we compared it with approaches that employ a robust estimator only in the HR image update and integrate a heuristic scheme for the step size.[22,24] We also compared several robust estimators in that framework: the truncated least squares (TLS), the Geman-McClure, and the Lorentzian error norms.

In all experiments, in order to have a first estimate of the HR image, an LR image was chosen at random and it was upscaled by bicubic interpolation. Convergence of the SR algorithm was achieved when $\|\hat{\mathbf{z}}^{n+1} - \hat{\mathbf{z}}^n\| / \|\hat{\mathbf{z}}^n\| < 10^{-5}$ or until 20 iterations were reached. The convergence of the iterative algorithm is guaranteed by the contraction mapping theorem.[30] According to this theorem, the iterative model

(a) (b) (c) (d)

Fig. 1 Representative frames of low-resolution images for (a) Susie, (b) Claire, (c) Helmet, and (d) Clock sequences.

Fig. 2 Reconstructed high-resolution images for 20 frames of the Susie sequence, with salt and pepper noise at 5%. (a) Robust parameters ε_k and $\alpha_k(\mathbf{z})$ and (b) no robust parameters.

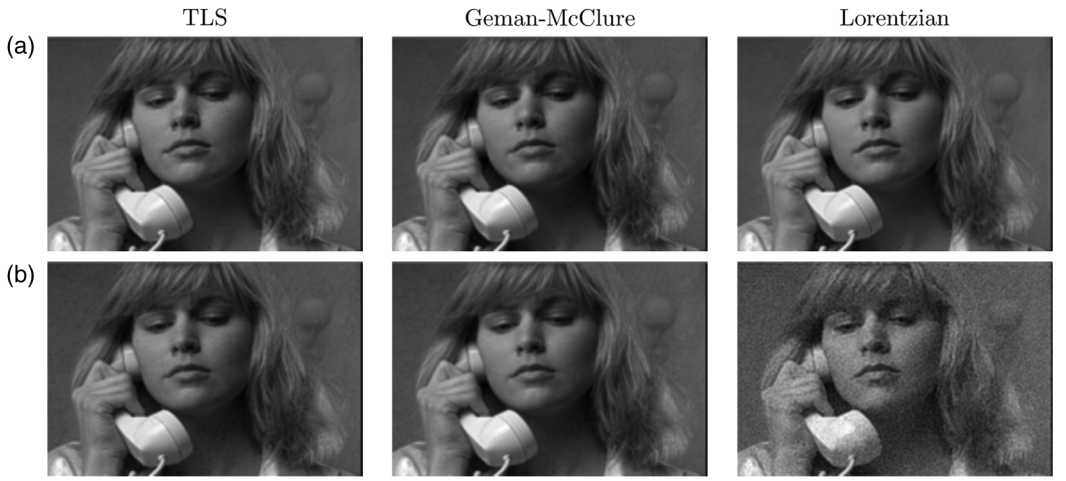

Fig. 3 Reconstructed high-resolution images for 20 frames of the Susie sequence, with salt and pepper noise at 10%. (a) Robust parameters ε_k and $\alpha_k(\mathbf{z})$ and (b) no robust parameters.

Table 1 Performance evaluation of the compared robust image super-resolution methods with respect to the peak signal-to-noise ratio (PSNR) (in decibels) for the reconstructed image Susie, with salt and pepper noise at 5 and 10%.

	Method in Ref. 22			Method in Ref. 24			Partially robust			Fully robust		
M-estimator	Mean	Std	Med	Mean	Std	Med	Mean	Std	Med	Mean	Std	Med
Salt and pepper at 5%												
Lorentzian	22.1	0.4	22.2	25.2	0.2	25.3	26.6	0.5	26.8	**27.2**	0.5	26.9
TLS	11.1	0.4	10.9	13.9	0.1	13.8	22.3	0.6	22.4	**26.7**	0.3	26.8
Geman	21.4	0.8	22.1	22.0	0.1	22.0	25.6	0.7	25.4	**26.6**	0.1	26.5
Salt and pepper at 10%												
Lorentzian	22.1	0.8	21.9	25.1	0.2	25.0	26.0	0.7	26.3	**26.9**	0.4	26.9
TLS	11.3	0.4	11.0	14.0	0.0	14.0	20.6	0.5	20.7	**25.9**	0.5	26.0
Geman	22.2	0.6	22.0	22.1	0.1	22.1	25.7	0.3	25.8	**25.4**	0.4	25.3

Note: TLS, truncated least squares.

Table 2 Performance evaluation of the compared robust image super-resolution methods with respect to the structural similarity (SSIM) statistics for the reconstructed image Susie, with salt and pepper noise at 5 and 10%.

	Method in Ref. 22			Method in Ref. 24			Partially robust			Fully robust		
M-estimator	Mean	Std	Med	Mean	Std	Med	Mean	Std	Med	Mean	Std	Med
Salt and pepper at 5%												
Lorentzian	0.7	0.0	0.7	0.7	0.0	0.7	0.6	0.0	0.6	**0.9**	0.0	0.9
TLS	0.2	0.0	0.2	0.4	0.0	0.4	0.7	0.0	0.7	**0.9**	0.0	0.9
Geman	0.6	0.1	0.6	0.7	0.0	0.7	0.7	0.0	0.7	**0.9**	0.0	0.9
Salt and pepper at 10%												
Lorentzian	0.7	0.0	0.7	0.8	0.0	0.8	0.6	0.0	0.6	**0.9**	0.0	0.9
TLS	0.3	0.0	0.3	0.4	0.0	0.4	0.7	0.1	0.8	**0.9**	0.0	0.9
Geman	0.7	0.0	0.7	0.8	0.0	0.8	0.8	0.0	0.8	**0.9**	0.0	0.9

[Eq. (5)] converges to a unique solution $\hat{\mathbf{z}}$. Therefore, our algorithm always converges.

A quantitative evaluation of the obtained HR images is given by the peak SNR (PSNR) defined by

$$\mathrm{PSNR} = 10\log_{10}\frac{255^2}{\|\mathbf{z}-\hat{\mathbf{z}}\|}, \tag{15}$$

where $\hat{\mathbf{z}}$ is the estimated HR image and $\mathbf{z}$ is the ground truth.

The structural similarity measure index (SSIM)[31] is a metric that represents a visual distortion between a reference image and the observe LR image. SSIM is regarded as a function between two images $\mathbf{z}$ and $\hat{\mathbf{z}}$ and it is expressed as

$$\mathrm{SSIM}(\mathbf{z},\hat{\mathbf{z}}) = \frac{(2\mu_{\mathbf{z}}\mu_{\hat{\mathbf{z}}}+C_1)(2\sigma_{\mathbf{z}\hat{\mathbf{z}}}+C_2)}{(\mu_{\mathbf{z}}^2+\mu_{\hat{\mathbf{z}}}^2+C_1)(\sigma_{\mathbf{z}}^2+\sigma_{\hat{\mathbf{z}}}^2+C_2)}, \tag{16}$$

where $\mu_{\mathbf{z}}$ and $\mu_{\hat{\mathbf{z}}}$ denote the mean intensity of the ground truth and the estimated HR image, respectively. $\sigma_{\mathbf{z}}$ and $\sigma_{\hat{\mathbf{z}}}$ are the standard deviations of the two images and C_1 and C_2 are constants added to avoid instability.

Finally, we have further used the visual information fidelity measure (VIF)[32] in order to assess the quality of the estimated HR image. It is a measure of statistical modeling that could ideally be extracted by the eye–brain system from nonoverlapping blocks in a wavelet subband in the HR and the reference images.

Table 3 Performance evaluation of the compared robust image super-resolution methods with respect to the visual information fidelity (VIF) statistics for the reconstructed image Susie, with salt and pepper noise at 5 and 10%.

	Method in Ref. 22			Method in Ref. 24			Partially robust			Fully robust		
M-estimator	Mean	Std	Med	Mean	Std	Med	Mean	Std	Med	Mean	Std	Med
Salt and pepper at 5%												
Lorentzian	0.6	0.0	0.6	0.8	0.0	0.8	0.5	0.0	0.5	**0.9**	0.0	0.9
TLS	0.1	0.0	0.1	0.1	0.0	0.1	0.8	0.1	0.8	**0.9**	0.0	0.9
Geman	0.1	0.0	0.5	0.8	0.0	0.8	0.8	0.0	0.8	**0.9**	0.0	0.9
Salt and pepper at 10%												
Lorentzian	0.6	0.0	0.5	0.8	0.0	0.8	0.5	0.0	0.5	**0.9**	0.0	0.9
TLS	0.1	0.0	0.1	0.1	0.0	0.1	0.7	0.1	0.7	**0.9**	0.0	0.9
Geman	0.5	0.0	0.5	0.8	0.0	0.8	0.8	0.0	0.8	**0.9**	0.0	0.9

Fig. 4 Reconstructed high-resolution images for 20 frames of the Claire sequence, with speckle noise at 1%. (a) Robust parameters ε_k and $\alpha_k(\mathbf{z})$ and (b) no robust parameters.

In the first set of experiments, 20 frames of the Susie sequence [Fig. 1(a)] were used and 50% of them were degraded by salt and pepper noise. Two cases were examined: corruption of 5 and 10% of the pixels in the respective frame. Figures 2(a) and 3(a) depict the reconstructed HR images of the fully robust image SR algorithm for this experiment using three different types of M-estimators (e.g., Lorentzian, Geman-McClure, and TLS) with 5 and 10% salt and pepper noise, respectively. In Figs. 2(b) and 3(b), the reconstructed HR images with a robust estimator employed only in the estimation of the HR image and not for the parameters ε_k^n and $\alpha_k(\mathbf{z})$ are shown.

Table 1 presents the statistics of PSNR for the proposed algorithm for 10 realizations of the experiment in each case. In this table, the term "partially robust" refers to the employment of a robust estimator only for the computation of the HR image using Eq. (10) but not for the parameters $\alpha_k(\mathbf{z})$ and ε_k^n, which were computed by Eqs. (4) and (6), respectively. The term "fully robust" indicates that a robust estimator was also employed for the computation of $\alpha_k(\mathbf{z})$ and ε_k^n, which were computed using Eqs. (9) and (11), respectively. PSNR values in bold indicate the best reconstructed HR image with respect to the robust estimator. In terms of PSNR, the proposed method achieves better reconstruction results with respect to the partially robust technique and the methods of El-Yamany and Papamichalis[22] and Patanavijit et al.[24] for all three robust M-estimators.

Table 2 shows the statistics using the SSIM index. Notice that the best performance is accomplished for the fully robust method. In Table 3, VIF statistics for the Susie sequence are shown. As can be seen, our method achieves better results for the TLS and the Geman-McClure estimator for 5% salt and pepper noise, while it is better than the other methods for 10% salt and pepper noise when the Lorentzian estimator

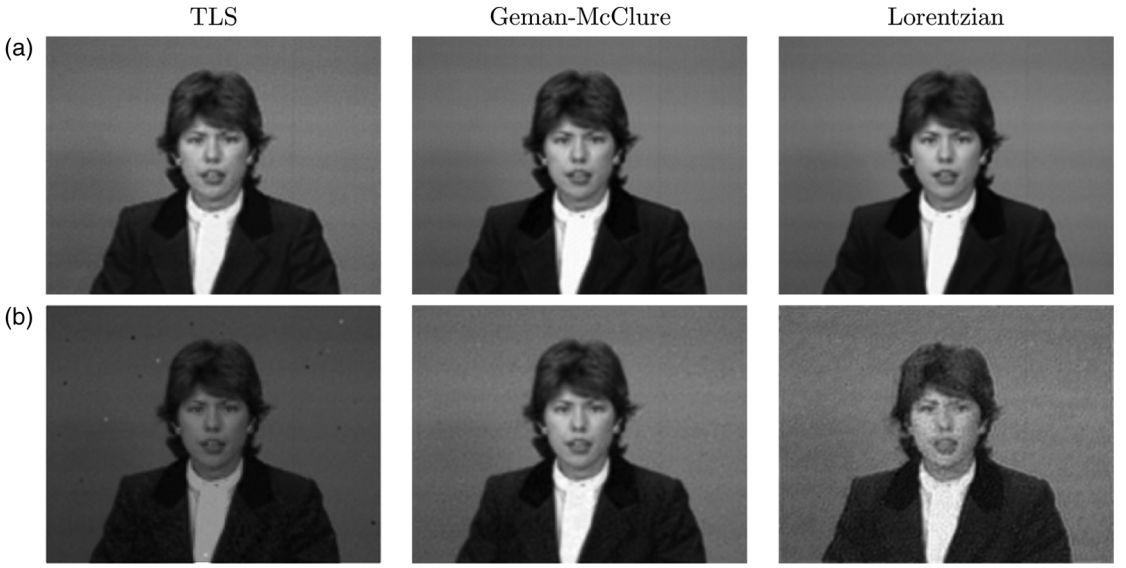

Fig. 5 Reconstructed high-resolution images for 20 frames of the Claire sequence, with speckle noise at 2%. (a) Robust parameters ε_k and $\alpha_k(\mathbf{z})$ and (b) no robust parameters.

Table 4 Performance evaluation of the compared robust image super-resolution methods with respect to PSNR (in decibels) for the reconstructed image Claire, with speckle noise at 1 and 2%.

	Method in Ref. 22			Method in Ref. 24			Partially robust			Fully robust		
M-estimator	Mean	Std	Med	Mean	Std	Med	Mean	Std	Med	Mean	Std	Med
						Speckle at 1%						
Lorentzian	22.3	0.5	22.3	27.8	0.1	27.8	23.3	0.4	23.3	**29.9**	0.1	30.5
TLS	10.4	0.3	10.3	11.5	0.1	11.5	16.9	0.6	16.8	**28.2**	0.6	28.3
Geman	21.6	0.8	21.3	23.2	0.16	23.2	29.0	0.4	29.0	**29.8**	0.5	30.0
						Speckle at 2%						
Lorentzian	22.6	0.7	22.7	27.9	0.1	27.9	22.2	0.8	22.6	**31.2**	0.8	31.5
TLS	10.5	0.1	10.5	11.5	0.1	11.5	14.3	0.5	14.0	**29.5**	0.5	29.4
Geman	21.6	0.5	21.5	23.2	0.1	23.1	28.8	0.6	29.4	**31.1**	0.2	31.1

is employed. The values in bold indicate the best reconstruction result with respect to the robust estimator. Notice that the TLS estimator underperforms when used with the methods of El-Yamany and Papamichalis[22] and Patanavijit et al.[24]

In the second set of experiments, 20 frames of the Claire sequence [Fig. 1(b)] were used, of which 50% were degraded by speckle noise. Speckle noise is a granular noise that downgrades the quality of an image. Let x_k be the image to which we want to add speckle noise. Then

$$y_k = x_k + n \times x_k, \tag{17}$$

where n is uniformly distributed random noise with zero mean and standard deviation σ_2 and y_k is the degraded LR image. Experiments have been conducted for 1 and 2% configurations of speckle noise in randomly selected LR image frames. In Figs. 4(a) and 5(a), the reconstructed HR images for the Claire sequence are shown, with speckle noise at 1 and 2%, using the proposed method. The reconstructed HR images for the same sequence and the same amount of noise using the partially robust technique are shown in Figs. 4(b) and 5(b). As can be observed, the fully robust method is able to fully wipe away speckle noise and reconstruct a clean image, while the partially robust method suffers from noise artifacts.

In Table 4, PSNR values for the reconstructed Claire sequence with speckle noise at 1 and 2% are shown. The robust variant is the most accurate SR method for all three M-estimators. Tables 5 and 6 present the SSIM and VIF

Table 5 Performance evaluation of the compared robust image super-resolution methods with respect to the SSIM statistics for the reconstructed image Claire, with speckle noise at 1 and 2%.

	Method in Ref. 22			Method in Ref. 24			Partially robust			Fully robust		
M-estimator	Mean	Std	Med	Mean	Std	Med	Mean	Std	Med	Mean	Std	Med
						Speckle at 1%						
Lorentzian	0.8	0.0	0.8	0.8	0.0	0.8	0.6	0.2	0.6	**0.9**	0.1	0.9
TLS	0.4	0.1	0.4	0.5	0.0	0.5	0.6	0.1	0.7	**0.9**	0.1	0.9
Geman	0.8	0.0	0.8	0.8	0.0	0.8	0.8	0.0	0.8	**0.9**	0.0	0.9
						Speckle at 2%						
Lorentzian	0.8	0.0	0.8	0.8	0.0	0.8	0.5	0.2	0.5	**0.9**	0.0	0.9
TLS	0.3	0.1	0.4	0.5	0.0	0.5	0.7	0.1	0.7	**0.7**	0.0	0.9
Geman	0.8	0.1	0.7	0.8	0.0	0.8	0.8	0.0	0.8	**0.9**	0.0	0.9

Table 6 Performance evaluation of the compared robust image super-resolution methods with respect to the VIF statistics for the reconstructed image Claire, with speckle noise at 1 and 2%.

	Method in Ref. 22			Method in Ref. 24			Partially robust			Fully robust		
M-estimator	Mean	Std	Med	Mean	Std	Med	Mean	Std	Med	Mean	Std	Med
						Speckle at 1%						
Lorentzian	0.3	0.0	0.3	0.7	0.0	0.7	0.4	0.1	0.4	**0.8**	0.2	0.8
TLS	0.1	0.0	0.1	0.1	0.0	0.1	0.3	0.1	0.3	**0.7**	0.1	0.7
Geman	0.3	0.2	0.2	0.6	0.0	0.6	0.6	0.0	0.6	**0.7**	0.1	0.8
						Speckle at 2%						
Lorentzian	0.4	0.0	0.4	0.7	0.0	0.7	0.3	0.1	0.3	**0.8**	0.1	0.8
TLS	0.1	0.0	0.1	0.1	0.0	0.1	0.4	0.2	0.4	**0.7**	0.0	0.7
Geman	0.3	0.0	0.3	0.7	0.0	0.7	0.7	0.0	0.7	**0.8**	0.0	0.8

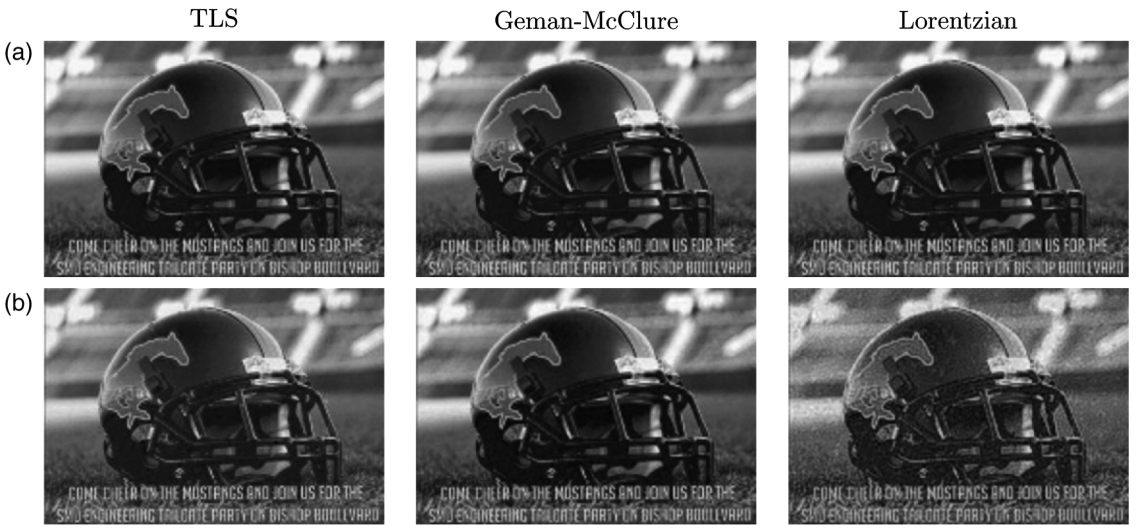

Fig. 6 Reconstructed high-resolution images for 20 frames of the Helmet sequence. (a) Robust parameters ε_k and $\alpha_k(\mathbf{z})$ and (b) no robust parameters.

Table 7 Performance evaluation of the compared robust image super-resolution methods with respect to PSNR (in decibels) for the reconstructed image Helmet.

	Method in Ref. 22			Method in Ref. 24			Partially robust			Fully robust		
M-estimator	Mean	Std	Med	Mean	Std	Med	Mean	Std	Med	Mean	Std	Med
Lorentzian	20.4	0.5	20.4	23.1	0.0	23.1	18.4	0.4	18.9	**23.8**	0.4	23.0
TLS	7.5	0.4	7.3	14.4	0.1	14.4	19.9	0.6	20.0	**23.0**	0.0	23.0
Geman	20.4	0.9	20.5	22.7	0.1	22.7	22.5	0.3	22.5	**23.0**	0.0	23.0

Table 8 Performance evaluation of the compared robust image super-resolution methods with respect to SSIM statistics for the reconstructed image Helmet.

	Method in Ref. 22			Method in Ref. 24			Partially robust			Fully robust		
M-estimator	Mean	Std	Med	Mean	Std	Med	Mean	Std	Med	Mean	Std	Med
Lorentzian	0.7	0.0	0.7	0.8	0.0	0.8	0.7	0.1	0.6	**0.9**	0.0	0.9
TLS	0.1	0.0	0.1	0.5	0.0	0.5	0.7	0.1	0.7	**0.8**	0.0	0.8
Geman	0.7	0.0	0.7	0.8	0.0	0.8	0.8	0.0	0.8	**0.9**	0.0	0.9

Table 9 Performance evaluation of the compared robust image super-resolution methods with respect to VIF statistics for the reconstructed image Helmet.

	Method in Ref. 22			Method in Ref. 24			Partially robust			Fully robust		
M-estimator	Mean	Std	Med	Mean	Std	Med	Mean	Std	Med	Mean	Std	Med
Lorentzian	0.7	0.0	0.7	0.7	0.0	0.7	0.5	0.1	0.5	**0.8**	0.1	0.8
TLS	0.2	0.0	0.2	0.4	0.0	0.4	0.6	0.1	0.6	**0.7**	0.0	0.7
Geman	0.7	0.1	0.7	0.7	0.0	0.7	0.7	0.0	0.7	**0.8**	0.0	0.8

statistics for the same sequence. As can be seen, the TLS estimator does not perform very well when associated with the El-Yamany and Papamichalis[22] and Patanavijit et al.[24] methods.

The third set of experiments contains a sequence of 10 LR frames depicting a football helmet [Fig. 1(c)]. In order to simulate motion errors, a global translational model is assumed. Thirty percent of randomly selected LR images were transformed by the translation of 15 pixels along the horizontal and vertical directions, while a rotation of 20 deg was also applied. The misalignment is large and the standard SR reconstruction methods cannot account for it without

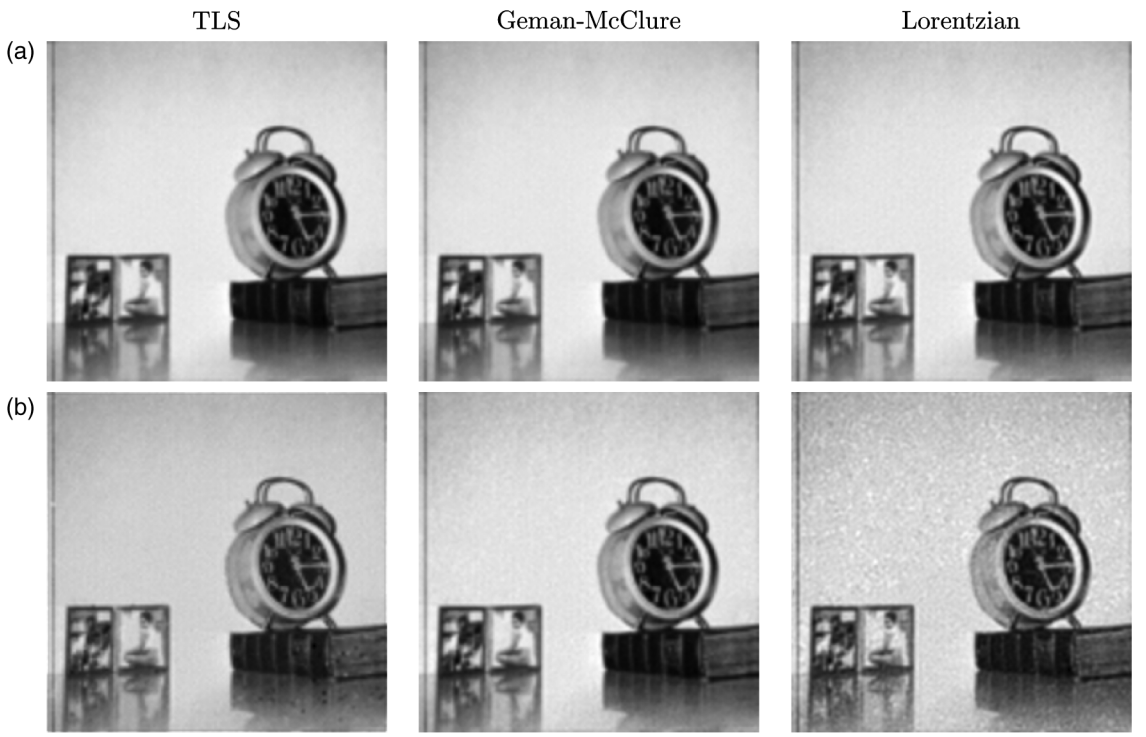

Fig. 7 Reconstructed high-resolution images for 20 frames of the Clock sequence. (a) Robust parameters ε_k and $\alpha_k(\mathbf{z})$ and (b) no robust parameters.

a robust estimator. The reconstructed HR images for the proposed method are depicted in Fig. 6(a) and those for the partially robust method are shown in Fig. 6(b). As can be seen, the proposed method can successfully suppress the effect of outliers, resulting in an image free of noise artifacts. On the other hand, the partially robust technique is of sightly lower quality.

Tables 7, 8, and 9 present the PSNR, SSIM index, and VIF numerical results, respectively, for this experiment comparing the proposed fully robust method against the partially robust version and the methods of El-Yamany and Papamichalis[22] and Patanavijit et al.[24] The values in bold indicate the best performance for the corresponding robust estimator. Notice that the proposed method performs better than the other methods in all experiments and the worst performance is achieved by the TLS estimator for all methods.

Finally, the fourth set of experiments consists of a sequence of seven LR frames [Fig. 1(d)]. In two out of seven consecutive frames, an object representing occlusion appears. Occlusion was intentionally added in order to simulate accidental changes in the scene and it is treated as an outlier by the method. The reconstructed HR images for the proposed method using the three M-estimators are illustrated in Fig. 7(a). Figure 7(b) depicts the reconstructed HR images when the partially robust approach is employed. As can be seen, there is a visible noise distortion in the reconstructed images, which is caused by the nonrobust computation of the parameters ε_k and $\alpha_k(\mathbf{z})$.

PSNR, SSIM index, and VIF statistic results are presented in Tables 10, 11, and 12, respectively. The values in bold represent the best performance for the corresponding robust estimator. Our method performs better in all experiments and is able to fully reconstruct an HR image, suppressing the outliers in the cases where partial occlusion is apparent in the LR images. For the method of El-Yamany and Papamichalis,[22] the least good estimator seems to be Geman-McClure, whereas for the method of Patanavijit et al.,[24] the least good estimator seems to be TLS. Let us recall that in all experiments involving the proposed method, the parameters ε_k and $\alpha_k(\mathbf{z})$ were robustly estimated and the outlier threshold was computed using the MAD criterion [Eq. (14)], thus suppressing many outliers which have

Table 10 Performance evaluation of the compared robust image super-resolution methods with respect to PSNR (in decibels) for the reconstructed image Clock.

	Method in Ref. 22			Method in Ref. 24			Partially robust			Fully robust		
M-estimator	Mean	Std	Med	Mean	Std	Med	Mean	Std	Med	Mean	Std	Med
Lorentzian	25.1	0.1	25.1	25.1	0.0	25.1	22.0	0.18	22.2	**25.8**	0.1	25.8
TLS	24.1	0.1	24.07	10.1	0.1	10.1	16.8	0.4	16.1	**24.8**	0.2	24.8
Geman	9.8	0.2	9.7	24.7	0.2	24.6	25.1	0.3	25.2	**25.2**	0.1	25.2

Table 11 Performance evaluation of the compared robust image super-resolution methods with respect to SSIM statistics for the reconstructed image Clock.

	Method in Ref. 22			Method in Ref. 24			Partially robust			Fully robust		
M-estimator	Mean	Std	Med	Mean	Std	Med	Mean	Std	Med	Mean	Std	Med
Lorentzian	0.8	0.0	0.8	0.8	0.0	0.8	0.7	0.0	0.7	**0.9**	0.0	0.9
TLS	0.8	0.0	0.8	0.7	0.0	0.7	0.7	0.2	0.7	**0.9**	0.0	0.9
Geman	0.5	0.0	0.5	0.8	0.0	0.8	0.8	0.0	0.8	**0.9**	0.0	0.9

Table 12 Performance evaluation of the compared robust image super-resolution methods with respect to VIF statistics for the reconstructed image Clock.

	Method in Ref. 22			Method in Ref. 24			Partially robust			Fully robust		
M-estimator	Mean	Std	Med	Mean	Std	Med	Mean	Std	Med	Mean	Std	Med
Lorentzian	0.7	0.0	0.7	0.7	0.0	0.7	0.7	0.0	0.7	**0.9**	0.0	0.9
TLS	0.7	0.0	0.7	0.3	0.0	0.3	0.5	0.2	0.5	**0.8**	0.0	0.8
Geman	0.2	0.0	0.2	0.7	0.0	0.7	0.7	0.0	0.7	**0.8**	0.0	0.8

occurred due to noise artifacts, misregistration errors, or occlusion.

5 Conclusions

In this paper, we presented a fully robust image SR algorithm where the estimation of the HR image was integrated in two steps. First, the regularization parameters were robustly estimated in an automatic manner, and then, the optimal step size of the update of the HR image was computed for every single LR frame. The outlier threshold was automatically estimated in a robust framework as the residual error between the estimation of the degraded HR image and the upscaled k'th LR frame. We demonstrated that under different assumptions and different M-estimators we can derive a powerful SR algorithm that suppresses the effect of outliers.

References

1. R. C. Hardie, K. J. Barnard, and E. E. Armstrong, "Joint MAP image registration and high-resolution image estimation using a sequence of undersampled images," *IEEE Trans. Image Process.* **6**(12), 1621–1633 (1997).
2. H. He and L. P. Kondi, "Resolution enhancement of video sequences with simultaneous estimation of the regularization parameter," *J. Electron. Imaging* **13**(3), 586–596 (2004).
3. H. He and L. P. Kondi, "An image super-resolution algorithm for different error levels per frame," *IEEE Trans. Image Process.* **15**(3), 592–603 (2006).
4. D. Capel and A. Zisserman, "Computer vision applied to super-resolution," *IEEE Signal Process. Mag.* **20**(3), 75–86 (2003).
5. G. K. Chantas, N. P. Galatsanos, and N. A. Woods, "Super-resolution based on fast registration and maximum a posteriori reconstruction," *IEEE Trans. Image Process.* **16**(7), 1821–1830 (2007).
6. T. Q. Pham, L. J. van Vliet, and K. Schutte, "Robust super-resolution without regularization," *J. Phys.* **124**(1), 012036 (2008).
7. L. C. Pickup et al., "Overcoming registration uncertainty in image super-resolution: maximize or marginalize?," *EURASIP J. Adv. Signal Process.* **2007**, 023565 (2007).
8. M. Vrigkas, C. Nikou, and L. P. Kondi, "On the improvement of image registration for high accuracy super-resolution," in *Proc. IEEE Int. Conf. on Acoustics, Speech and Signal Processing*, pp. 981–984, IEEE, Prague, Czech Republic (2011).
9. F. Šroubek and J. Flusser, "Resolution enhancement via probabilistic deconvolution of multiple degraded images," *Pattern Recognit. Lett.* **27**(4), 287–293 (2006).
10. S. Farsiu, M. Elad, and P. Milanfar, "Multi-frame demosaicing and super-resolution of color images," *IEEE Trans. Image Process.* **15**(1), 141–159 (2006).
11. A. Kanemura, S. Maeda, and S. Ishii, "Edge-preserving Bayesian image superresolution based on compound Markov random fields," in *Proc. 17th Int. Conf. on Artificial Neural Networks*, pp. 611–620, Springer, Porto, Portugal (2007).
12. L. C. Pickup et al., "Bayesian image super-resolution, continued," in *Proc. Advances in Neural Information Processing Systems*, pp. 1089–1096, MIT Press, Vancouver, British Columbia, Canada (2006).
13. C. A. Segall et al., "Bayesian resolution enhancement of compressed video," *IEEE Trans. Image Process.* **13**(7), 898–911 (2004).
14. M. E. Tipping and C. M. Bishop, "Bayesian image super-resolution," in *Proc. Advances in Neural Information Processing Systems*, pp. 1303–1310, MIT Press, Vancouver, British Columbia, Canada (2003).
15. E. Bilgazyev et al., "Improved face recognition using super-resolution," in *Proc. Int. Joint Conf. on Biometrics*, pp. 1–7, IEEE, New Delhi, India (2011).
16. S. Baker and T. Kanade, "H. faces," in *4th IEEE Int. Conf. on Automatic Face and Gesture Recognition*, pp. 83–89, IEEE Computer Society, Grenoble, France (2000).
17. M. F. Tappen and C. Liu, "A Bayesian approach to alignment-based image hallucination," in *Proc. European Conf. on Computer Vision*, pp. 236–249, Springer, Florence, Italy (2012).
18. S. Berretti, A. D. Bimbo, and P. Pala, "Superfaces: a super-resolution model for 3D faces," in *Proc. European Conf. on Computer Vision*, pp. 73–82, Springer, Florence, Italy (2012).
19. A. Zomet, A. Rav-Acha, and S. Peleg, "Robust super-resolution," in *Proc. IEEE Workshop on Applications of Computer Vision*, Vol. 1, pp. 645–650, IEEE Computer Society, Kauai, Hawaii (2001).
20. N. A. El-Yamany and P. E. Papamichalis, "Using bounded-influence M-estimators in multi-frame super-resolution reconstruction: a comparative study," in *Proc. 15th IEEE Int. Conf. on Image Processing*, pp. 337–340, IEEE, San Diego, California (2008).
21. N. A. El-Yamany and P. E. Papamichalis, "An adaptive M-estimation framework for robust image superresolution without regularization," *Proc. SPIE* **6822**, 68221D (2008).
22. N. A. El-Yamany and P. E. Papamichalis, "Robust color image super-resolution: an adaptive M-estimation framework," *EURASIP J. Image Video Process.* **2008**, 763254 (2008).
23. M. D. Robinson, C. A. T. J. Y. Lo, and S. Farsiu, "Efficient Fourier-wavelet super-resolution," *IEEE Trans. Image Process.* **19**(10), 2669–2681 (2010).
24. V. Patanavijit, S. Tae-O-Sot, and S. Jitapunkul, "A Lorentzian stohastic estimation for a robust iterative multiframe super-resolution reconstruction with Lorentzian-Tikhonov regularization," *EURASIP J. Adv. Signal Process.* **2007**, 034821 (2007).
25. V. Patanavijit, S. Tae-O-Sot, and S. Jitapunkul, "A robust iterative superresolution reconstruction of image sequences using a Lorentzian Bayesian approach with fast affine block-based registration," in *Proc. IEEE Int. Conf. on Image Processing*, Vol. 5, pp. 393–396, IEEE, San Antonio, Texas (2007).
26. M. Tanaka, Y. Yaguchi, and M. Okutomi, "Robust and accurate estimation of multiple motions for whole-image super-resolution," in *Proc. IEEE Int. Conf. on Image Processing*, pp. 649–652, IEEE, San Diego, California (2008).
27. S. Farsiu et al., "Fast and robust multiframe super resolution," *IEEE Trans. Image Process.* **13**(10), 1327–1344 (2004).
28. M. Vrigkas, C. Nikou, and L. P. Kondi, "A fully robust framework for MAP image super-resolution," in *Proc. IEEE Int. Conf. on Image Processing*, pp. 2225–2228, IEEE, Lake Buena Vista, Orlando, Florida (2012).
29. P. J. Rousseeuw and A. M. Leory, *Robust Regression and Outlier Detection*, John Wiley & Sons, New York, New York (1987).
30. A. K. Katsaggelos, "Iterative image restoration algorithms," *Opt. Eng.* **28**(7), 735–748 (1989).
31. Z. Wang et al., "Image quality assessment: from error visibility to structural similarity," *IEEE Trans. Image Process.* **13**(4), 600–612 (2004).
32. H. R. Sheikh and A. C. Bovik, "Image information and visual quality," *IEEE Trans. Image Process.* **15**(2), 430–444 (2006).

Michalis Vrigkas received his BSc and MSc in computer science from the University of Ioannina, Greece, in 2008 and 2010, respectively. He is currently pursuing his PhD degree in the Department of Computer Science and Engineering, University of Ioannina, Greece. He has participated in several EC-funded ICT projects. His research interests include image processing and analysis, computer vision, machine learning, and pattern recognition.

Christophoros Nikou received the Diploma in electrical engineering from Aristotle University of Thessaloniki, Greece, in 1994 and the DEA and PhD degrees in image processing and computer vision from Louis Pasteur University, Strasbourg, France, in 1995 and 1999, respectively. Since 2013 he has been an associate professor with the Department of Computer Science and Engineering, University of Ioannina, Ioannina, Greece. His research interests mainly include image processing and analysis, computer vision and pattern recognition and their application to medical imaging.

Lisimachos P. Kondi received the Diploma in electrical engineering from the Aristotle University of Thessaloniki, Greece, in 1994 and the MS and PhD degrees in electrical and computer engineering from Northwestern University, Evanston, IL, in 1996 and 1999, respectively. He is currently an associate professor with the Department of Computer Science and Engineering, University of Ioannina, Greece. His research interests are in the general areas of signal and image processing and communications, including image and video compression and transmission over wireless channels and the Internet, sparse models and compressive sensing, super-resolution of video sequences, and shape coding.